Focal Structure–Function Relationships in Primary Open-Angle Glaucoma Using OCT and OCT-A Measurements

Damon Wong,[1–3] Jacqueline Chua,[3,4] Emily Lin,[3] Bingyao Tan,[1–3] Xinwen Yao,[1–3] Rachel Chong,[3] Chelvin Sng,[3,5] Amanda Lau,[3] Rahat Husain,[3] Tin Aung,[3,4,6] and Leopold Schmetterer[1,3,7–10]

[1]SERI-NTU Advanced Ocular Engineering (STANCE), Singapore
[2]NTU Institute of Health Technologies, Singapore
[3]Singapore Eye Research Institute, Singapore National Eye Centre, Singapore
[4]Academic Clinical Program, Duke-NUS Medical School, Singapore
[5]Ophthalmology Department, National University Hospital, Singapore
[6]Department of Ophthalmology, Yong Loo Lin School of Medicine, National University of Singapore, Singapore
[7]School of Chemical and Biomedical Engineering, Nanyang Technological University, Singapore
[8]Department of Clinical Pharmacology, Medical University of Vienna, Vienna, Austria
[9]Center for Medical Physics and Biomedical Engineering, Medical University of Vienna, Vienna, Austria
[10]Institute of Molecular and Clinical Ophthalmology, Basel, Switzerland

Correspondence: Leopold Schmetterer, Singapore Eye Research Institute, Singapore National Eye Centre, 20 College Road, The Academia, Level 6, Discovery Tower, Singapore 169856, Singapore; leopold.schmetterer@seri.com.sg.

Received: August 6, 2020
Accepted: November 30, 2020
Published: December 29, 2020

Citation: Wong D, Chua J, Lin E, et al. Focal structure–function relationships in primary open-angle glaucoma using OCT and OCT-A measurements. *Invest Ophthalmol Vis Sci*. 2020;61(14):33. https://doi.org/10.1167/iovs.61.14.33

Purpose. To evaluate the focal structure–function associations among visual field (VF) loss, optical coherence tomography angiography (OCT-A) vascular measurements, and optical coherence tomography (OCT) structural measurements in glaucoma.

Methods. In this cross-sectional study, subjects underwent standard automated perimetry, OCT-based nerve fiber thickness measurements, and OCT-A imaging. Mappings of focal VF test locations with OCT and OCT-A measurements were defined using anatomically adjusted nerve fiber trajectories and were studied using multivariate mixed-effects analysis. Segmented regression analysis was used to determine the presence of breakpoints in the structure–function associations.

Results. The study included 119 eyes from 86 Chinese subjects with primary open-angle glaucoma (POAG). VF mean deviation was significantly associated with global capillary perfusion density ($\beta = 0.13 \pm 0.08$) and global retinal nerve fiber layer thickness ($\beta = 0.09 \pm 0.02$). Focal capillary density (FCD) was significantly associated with VF losses at 34 VF test locations (66.7% of 24-2 VF), with 24 of the 34 locations being within 20° of retinal eccentricity. Focal nerve layer (FNL) thickness was significantly associated with 16 VF test locations (31.4% of 24-2 VF; eight locations within 20° eccentricity). For VF test locations in the central 10° VF, VF losses below the breakpoint were significantly associated with FCD (slope, 0.89 ± 0.12, $P < 0.001$), but not with FNL thickness (slope, 0.57 ± 0.39, $P = 0.15$).

Conclusions. Focal capillary densities were significantly associated with a wider range of visual field losses and in a larger proportion of the visual field compared to nerve fiber thickness.

Keywords: structure–function, OCT, OCTA, visual field

Glaucoma, one of the leading causes of blindness worldwide,[1,2] is a disease of the optic nerve characterized by progressive loss of retinal ganglion cells and their axons, leading to structural changes in the optic nerve head and loss of visual function. A structure–function relationship in glaucoma has been previously demonstrated by associating changes in the visual field (VF) with optical coherence tomography (OCT)-based retinal nerve fiber layer (RNFL) thickness measurements.[3–9]

Optical coherence tomography angiography (OCT-A) is a recent technique that allows in vivo visualization of ocular perfusion.[10–13] Recent OCT-A studies have shown reduced peripapillary and macular measurements in eyes with glaucoma[8,14–18] which can be attributed to reduced ocular perfusion.[19,20] These studies have shown that the floor effects exhibited by OCT-based RNFL parameters, in which increasing VF losses correspond poorly to detectable changes in the measured RNFL thickness, are largely absent from vascular OCT-A parameters. Spatial correlations have also been demonstrated between defects in the VF and vascular density in the corresponding peripapillary regions, using models defined based on hemispherical regions[21–23]

or sectors[24–27] from the Garway–Heath map.[28] However, an evaluation of the focal relationships between VF losses and structural and microvasculature measurements at each VF test point has yet to be reported.

The purpose of this study was to investigate the relationships between focal VF loss at individual test locations based on standard automated perimetry and capillary densities from OCT-A and RNFL thickness measurements from OCT by using a nerve fiber trajectory tracing model in eyes with glaucoma.

Methods

Subjects

In this cross-sectional study, subjects with primary open-angle glaucoma (POAG) were consecutively recruited from the Singapore National Eye Centre, a tertiary eye care institution in Singapore, from July 2018 to June 2019. These subjects were participants in the Singapore Eye Imaging Network, a clinical study designed to evaluate microvascular defects and their association with ocular conditions. Informed consent was obtained from all participants. The SingHealth Centralized Institutional Review Board approved all protocols, and all methods adhered to the tenets of the Declaration of Helsinki.

All participants underwent a comprehensive examination, including assessment of best-corrected visual acuity using a logarithm of minimum angle of resolution (logMAR) chart (Lighthouse International, New York, NY, USA), autorefractometry, intraocular pressure (IOP) measurement using Goldman applanation tonometry, and OCT and OCT-A imaging. Demographic data and medical history were obtained from case notes. Pupils were dilated with a drop of Gutt Mydriacyl (1% tropicamide) drops prior to imaging. Visual fields were assessed using standard automated perimetry (Humphrey Field Analyzer with Swedish Interactive Threshold Algorithm Fast 24-2; Carl Zeiss Meditec, Inc., Dublin, CA, USA). The test was considered reliable if fixation losses were less than 33% and false-positive and false-negative errors were less than 20%.

POAG eyes were defined based on clinical diagnosis, which included the presence of glaucomatous optic neuropathy (defined as loss of neuroretinal rim with a vertical cup:disc ratio of >0.7 or an inter-eye asymmetry of >0.2 and/or notching attributable to glaucoma) with compatible VF loss, open angles on gonioscopy, glaucoma hemifield test outside normal limits, and absence of secondary causes of glaucomatous optic neuropathy.

OCT Circumpapillary RNFL Analysis

RNFL analysis was performed using spectral-domain OCT imaging (Cirrus HD-OCT 5000; Carl Zeiss Meditec) with a 200 × 200 optic disc scan protocol. The circumpapillary RNFL thickness profile was automatically obtained from the in-built review software based on a 3.46-mm-diameter ring centered on the optic disc.

OCT-A Image Acquisition

OCT-A images were obtained using a commercial swept-source OCT system (PLEX Elite 9000; Carl Zeiss Meditec), which features a swept-source laser with a tunable center wavelength ranging from 1040 to 1060 nm and an A-scan rate of 100 kHz. Each eye underwent a 6 × 6-mm imaging protocol centered at the optic disc and a widefield 12 × 12-mm imaging protocol centered at the fovea. Depth-resolved angiographic signals were obtained using an optical microangiography technique that utilized both intensity and phase information.[29] The superficial capillary plexus (SCP) was obtained using the PLEX Elite 9000 built-in automated OCT layer segmentation, which identified and isolated angiographic signals in the slab defined by the inner limiting membrane and inner plexiform layer. En face OCT-A images generated from maximum projection of the SCP were extracted for further analysis. Positions of the optic discs were manually annotated based on the center of the optic disc margins on the widefield and optic disc structural OCT images, and the macular center was annotated as the center of the foveal avascular zone from the widefield OCT-A scan. Eyes in which the position of the optic disc in the 6 × 6-mm scan was more than 0.6 mm from the image center were excluded. Image quality checks were manually conducted to exclude images with signal strengths less than 6 or of poor quality. Regions in the OCT-A images due to artifacts observed in the corresponding OCT scans were also localized and omitted.

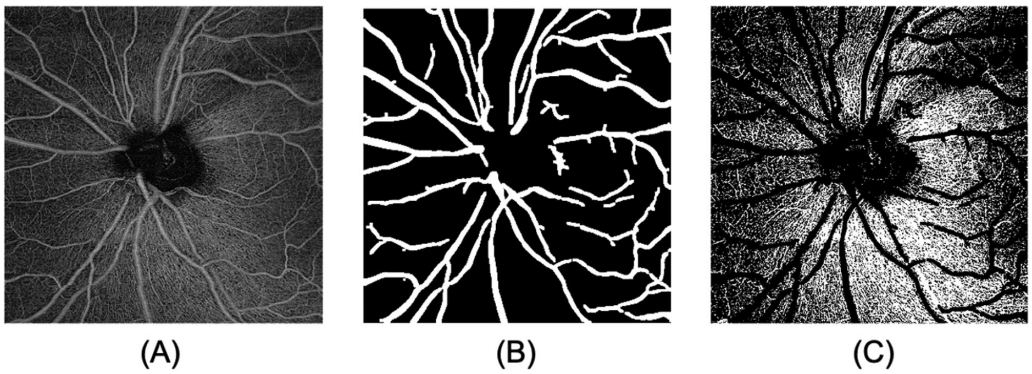

Figure 1. OCT-A image processing. (**A**) OCT-A images of the superficial plexus were acquired using a 6 × 6-mm optic nerve head protocol. (**B**) Major vessels were detected using a Hessian-based filter followed by adaptive thresholding. These major vessels were excluded from the OCT-A image to remove the contributions from the larger vessels. (**C**) After large vessel removal, global thresholding was applied to the OCT-A image to generate a binarized capillary map.

Investigative Ophthalmology & Visual Science

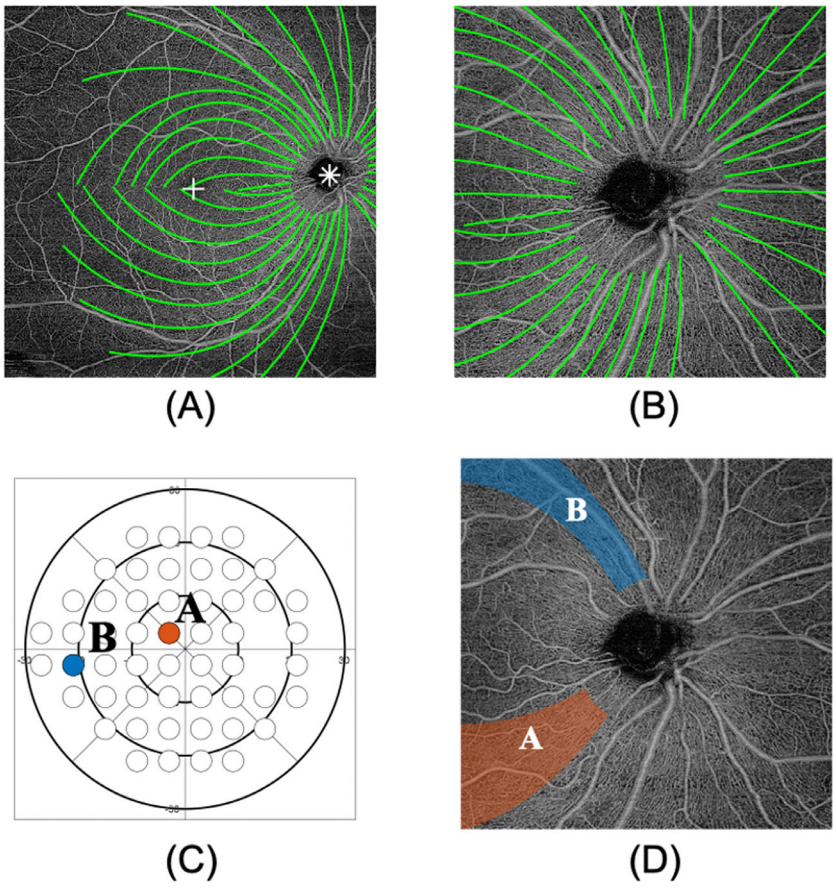

Figure 2. Illustration of the mapping protocol used in this study. (**A**) Using the locations of the optic nerve head (*asterisk*) and fovea (*cross*) as reference points, the individual nerve fiber trajectories were traced using the fiber trajectory tracing model.[31,32] (**B**) The tracings were then transferred onto the OCT-A image acquired with the 6 × 6-mm optic nerve head protocol. For each VF test point, the corresponding 95% limits of the fiber trajectories were used to demarcate a region of interest for calculation of the focal capillary density metrics. (**C**, **D**) An example of the mapping for the two VF points (**A**, *red*; **B**, *blue*) is shown. Mappings for all of the VF points with the corresponding nerve fiber trajectories are provided in the Supplementary Material.

OCT-A Image Processing

The optic nerve head OCT-A images (1024 × 1024 pixels) were processed using a customized MATLAB algorithm (MathWorks, Natick, MA, USA). Each OCT-A image underwent thresholding using a globally defined threshold that minimized the intra-class variance between pixels corresponding to vasculature and non-vasculature pixels, generating a binarized vasculature segmentation containing both capillaries and major blood vessels. To remove the major blood vessels, a separate Hessian-based filter proposed by Frangi et al.[30] was first applied on the OCT-A image, enhancing the major vessels while suppressing capillaries. Local adaptive thresholding using the mean intensity around the 128 × 128 neighborhood of each pixel was then applied to generate a binary mask of the major blood vessels. Finally, a capillary map was generated from the vasculature segmentation by removing pixels corresponding to the detected major blood vessels. An example of the image processing is shown in Figure 1.

Nerve Fiber Trajectory Model

We applied the nerve fiber trajectory model developed by Jansonius and colleagues.[31,32] Briefly, the model is a mathematical description of the nerve fiber trajectories in the retina originating from the optic disc, and it associates each test location of the VF with a range of fiber trajectories. The model has also been proposed as an approach for detecting glaucomatous progression.[33] To adapt the model for each of the eyes in the study, the calculated disc–foveal distances and disc–foveal angles based on the manual annotations were used to adjust the nerve fiber trajectories for each eye and were aligned with the location of the optic disc in the 6 × 6 mm OCT-A image. Figure 2 illustrates the aligned nerve fiber trajectory tracings overlaid on both optic disc and wide-field OCT-A scans.

Focal Analysis

From the nerve fiber trajectory model, each of the VF test locations was associated with a range of trajectories.[31] In our focal analysis, we used the 95% confidence interval range of nerve fiber trajectories, which were traced from the optic disc circumference to the image margin, to define the wedge-shaped region of interest (ROI) for each VF test location. This ROI represents the nerve fiber bundle or wedge associated with the test point based on the model. Examples of two VF test locations and the associated ROIs on the OCT-A image are shown in Figure 2. Detailed mappings

Investigative Ophthalmology & Visual Science

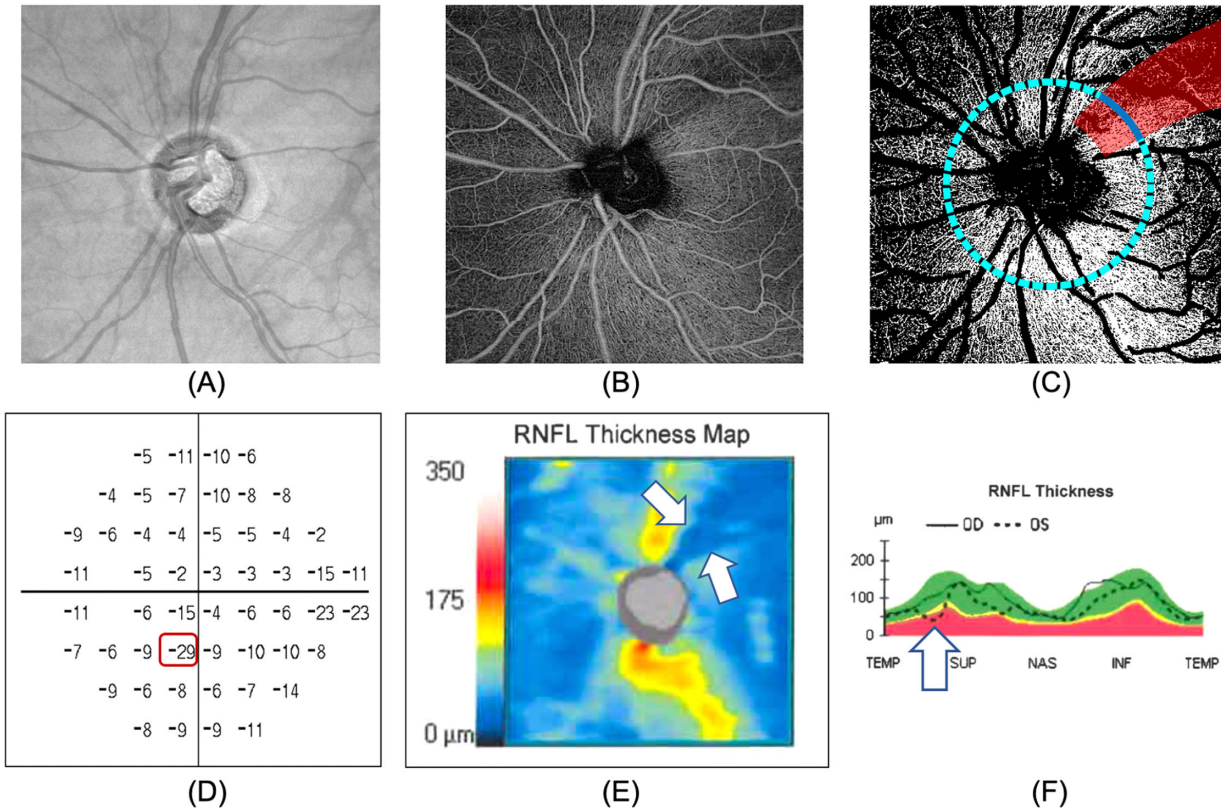

Figure 3. Focal relationship among VF loss, FCD, and FNL thickness. OCT (**A**) and OCT-A (**B**) images of the left eye (OS) of a subject are shown. (**C**) FCD region (*red zone*) on the OCT-A image corresponding to the VF defect at the test position indicated in (**D**). The region was defined by the nerve fiber trajectories. Decreased capillary density was observed within the FCD region. FNL thickness was defined by the arc (*blue*) on the circumpapillary RNFL (*dotted cyan circle*) bounded by the same nerve fiber trajectories as FCD. The extracted RNFL thickness map (**E**) and profile (**F**) show corresponding RNFL thinning (*white arrows*).

for all of the test locations in the 24-2 VF are provided in Supplementary Figure S1. Illustrations of the wedges defined by the nerve fibre tracings for each visual field test location are also provided in the Supplementary Video. Using the ROI for each test location, the focal capillary density (FCD) was calculated as the proportion of the ROI area occupied by capillaries. In addition, the average thickness corresponding to the arc of the circumpapillary RNFL profile within the focal ROI was computed as the focal nerve layer (FNL) thickness. This enabled a focal vascular–structural–function analysis through the association of a functional VF loss with a corresponding focal vascular perfusion metric (FCD) and focal structural metric (FNL thickness). Figure 3 shows an example of the focal structure mapping, together with the OCT and OCT-A images, the VF deviation map, the RNFL thickness map, and the measured circumpapillary RNFL thickness; the FCD region (red) and FNL thickness arc (blue) in the figure correspond to the indicated VF test location of the subject.

Table 1. Demographic Characteristics of the Study Subjects (119 Eyes, 86 Subjects)

Characteristic	Value
Age (y)	65.6 ± 12.2
Gender (female:male)	25:61
Ethnicity	Chinese
Refractive error (D)	–1.14 ± 1.95
VF MD (dB)	–3.56 ± 3.01
Intraocular pressure (mm Hg)	14.38 ± 2.75
Global RNFL thickness (µm)	74.02 ± 9.56
Global capillary density (%)	35.45 ± 7.77
Disc–fovea angle* (°)	9.52 ± 3.89
Disc–fovea distance† (mm)	4.47 ± 0.26

*Angle between the optic disc center and the foveola, with respect to the horizontal.
†Distance between the optic disc center and the foveola.

Statistical Analysis

The association between VF mean deviation (MD) and global capillary density, global RNFL thickness, and other global parameters was modeled using multivariate regression. As measurements from both eyes of a subject may be highly correlated, mixed-effects modeling was used to account for inter-eye correlations by adding a subject-specific random effect, with the other parameters of interest serving as fixed effects. Focal relationships at each VF test location were also individually modeled using mixed-effects regression, with the focal VF deviation values as the dependent variable and significant parameters from the global regression analysis as the independent variables.

Relationships between focal VF loss and the individual FNL thickness or FCD parameters were compared using two methods. Segmented regression (SR) analysis is an approach

Investigative Ophthalmology & Visual Science

Table 2. Multivariate Mixed-Effects Model for Global Factors Associated with VF MD

Factor	Regression Coefficient	95% Confidence Interval	P*
Age	0.01 ± 0.02	−0.04 to 0.06	0.791
Gender (female)	0.35 ± 0.60	−0.82 to 1.53	0.553
Refractive error	−0.11 ± 0.14	−0.38 to 0.17	0.445
Intraocular pressure	0.13 ± 0.08	−0.03 to 0.29	0.122
Global RNFL thickness	0.09 ± 0.02	0.05 to 0.13	**<0.001**
Global capillary density	0.13 ± 0.03	0.06 to 0.19	**<0.001**
Disc–fovea angle	0.09 ± 0.04	0.01 to 0.18	**0.034**
Disc–fovea distance	0.32 ± 0.87	−1.38 to 2.02	0.709

*P value indicates significance of coefficient; bolded values are statistically significant.

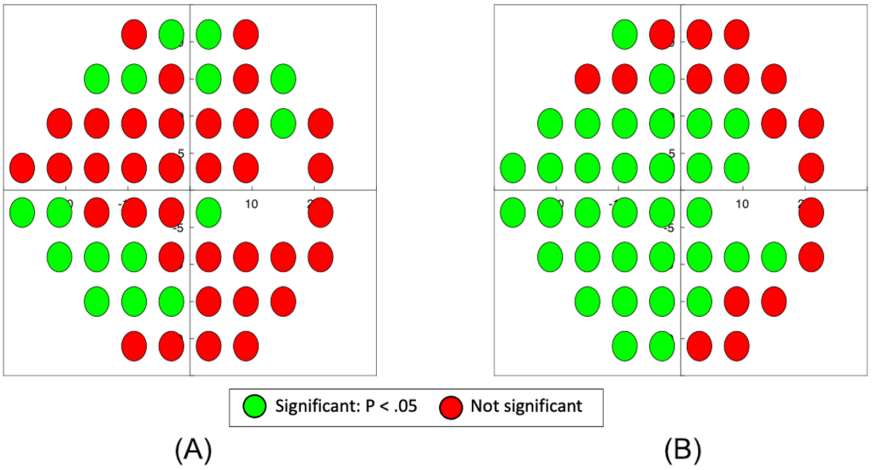

Figure 4. Significance of factors from the multivariate mixed-effects modeling at test points from the 24-2 VF for (**A**) focal RNFL thickness and (**B**) focal capillary perfusion density. *Green* indicates a test location in which the corresponding parameter was significantly associated with VF loss. Locations located nearer fixation (0°, 0°) were more significantly influenced by FCD than FNL thickness. Correlations for nasal VF test locations were poor for both FNL thickness and FCD. One VF test location at eccentricity (9°, −3°) was excluded due to the limited arc of the FNL thickness defined by the trajectories for that location.

that determines the breakpoint at which a change in slope occurs and has been used to investigate structure–function associations.[6,7] An estimate of the breakpoint was first determined using the Davies test,[34] which was then used as an initial value to simultaneously obtain the optimal breakpoint and the resulting slopes above and below the breakpoint. In this study, we defined a floor-like effect as a non-significant slope of the curve below the breakpoint. Locally weighted scatterplot smoothing (LOWESS) curves, which can be used to estimate a curve without assumptions of the underlying model, were also used to visually evaluate the relationships. Only VF test locations with deviation values < 0 decibel (dB) were used in the modeling.[3] All statistical analyses were carried out using Stata 13.1 (StataCorp, College Station, TX, USA) and the R platform (R Foundation for Statistical Computing, Vienna, Austria), with the segmented package. P values less than 0.05 were considered to be statistically significant.

Results

This study recruited 182 eyes of 114 Chinese subjects with POAG. After excluding 15 eyes with high myopia (SE < −6), 16 eyes for poor VF reliability, and 32 eyes due to poor OCT-A image quality, a total of 119 eyes from 86 subjects were included for analysis. The mean age of the subjects was 65.6 ± 12.2 years, and the subjects had an average VF mean deviation of −3.56 ± 3.01 dB. Demographic characteristics of the study patients are presented in Table 1.

Multivariate mixed-effects regression modeling was performed with VF MD as the dependent variable and global RNFL thickness, global capillary density (GCD), IOP, age, gender, refractive error, disc–fovea angle, disc area ratio, and disc–fovea distance as independent variables. Results of the regression model can be found in Table 2. A reduced global RNFL thickness ($\beta = 0.09$, $P < 0.001$), lower global capillary density ($\beta = 0.13$, $P < 0.001$), and larger angle between the disc and fovea ($\beta = 0.09$, $P < 0.001$) were associated with greater VF MD. All other variables were not significant.

Focal VF loss at each VF test location was individually modeled using multivariate mixed-effects regression, with FNL thickness, FCD, and disc–fovea angle as the independent variables. Full results of the regression analysis for each of the 24-2 VF test locations are provided in Supplementary Table S1. FCD was found to be significantly associated with VF loss in 34 of the 51 test locations (66.7%), whereas FNL thickness was significantly associated in 16 of the 51 test locations (31.4%). Figure 4 provides a visual representation of the significance of the regression coefficients for FNL thickness and FCD overlaid on the corresponding VF test locations. Table 3 provides the number of VF test locations with significant associations between focal VF loss and the corresponding FCD or FNL thickness metrics with respect to retinal eccentricity. The results indicate that FCD was signifi-

Table 3. Number of VF Test Locations with Significant Associations Between Focal VF Loss and FCD or FNL Thickness

Retinal Eccentricity*	FCD	FNL	VF Test Locations†
All	34 (66.7%)	16 (31.4%)	51
Less than 10°	11 (100.0%)	1 (9.1%)	11
Between 10° and 20°	13 (72.2%)	7 (38.9%)	18
More than 20°	10 (45.5%)	8 (36.3%)	22

Percentages in parentheses indicate the proportion of VF test locations with significant associations between VF loss and FCD or FNL against the total number of VF locations.

* Retinal eccentricity with respect to fixation.

† Total number of visual field test locations with respect to fixation based on the Humphrey 24-2 test.

cantly associated with focal VF loss in more VF test locations compared to FNL nearer to fixation.

Scatterplots of focal VF against FCD and FNL thickness within each of the three eccentricity regions (<10°, 10°–20°, >20°) are shown in Figure 5, together with the relationships modeled from the SR and LOWESS approaches, which were similar. From the plots, it can be seen that the relationships between VF loss and FCD or FNL thickness differ according to retinal eccentricity. Results from the SR analysis are presented in Table 4. Detected breakpoints were significant ($P < 0.05$) using the Davies test for both FCD and FNL thickness in all zones, except for FCD within 10° of fixation. Within the central 10°, the slope below the breakpoint for FNL thickness was not significant ($P = 0.18$), suggesting a floor-like effect beyond which increasing VF severity was not significantly associated with changes in nerve fiber thickness.

Discussion

In this study, we show that perfused capillary density in the superficial peripapillary region was significantly associated with overall severity of VF loss and with focal VF losses at a majority of VF test locations. Increased VF mean deviation was associated with decreased GCD and decreased global RNFL thickness. VF test locations in which VF losses were significantly associated with capillary density tended toward the central retina. A floor-like effect was observed for nerve fiber thicknesses with increasing VF losses within 10° of fixation but was not observed for the corresponding capillary densities.

To our knowledge, this is the first study in which an anatomical model of nerve fiber trajectories has been used to define focal regions of perfused capillary densities associated with individual VF test locations in glaucoma using OCT-A. Previous studies have evaluated the spatial correspondence of VF sensitivities with OCT-A at different levels of granularity. VF MD[18,35–37] has been shown to be well-associated with global, annular, or quadrant-based measures of vascular parameters in the circumpapillary region. Single hemifield analysis by associating VF losses from one VF hemifield with the corresponding OCT-A hemifield has also been

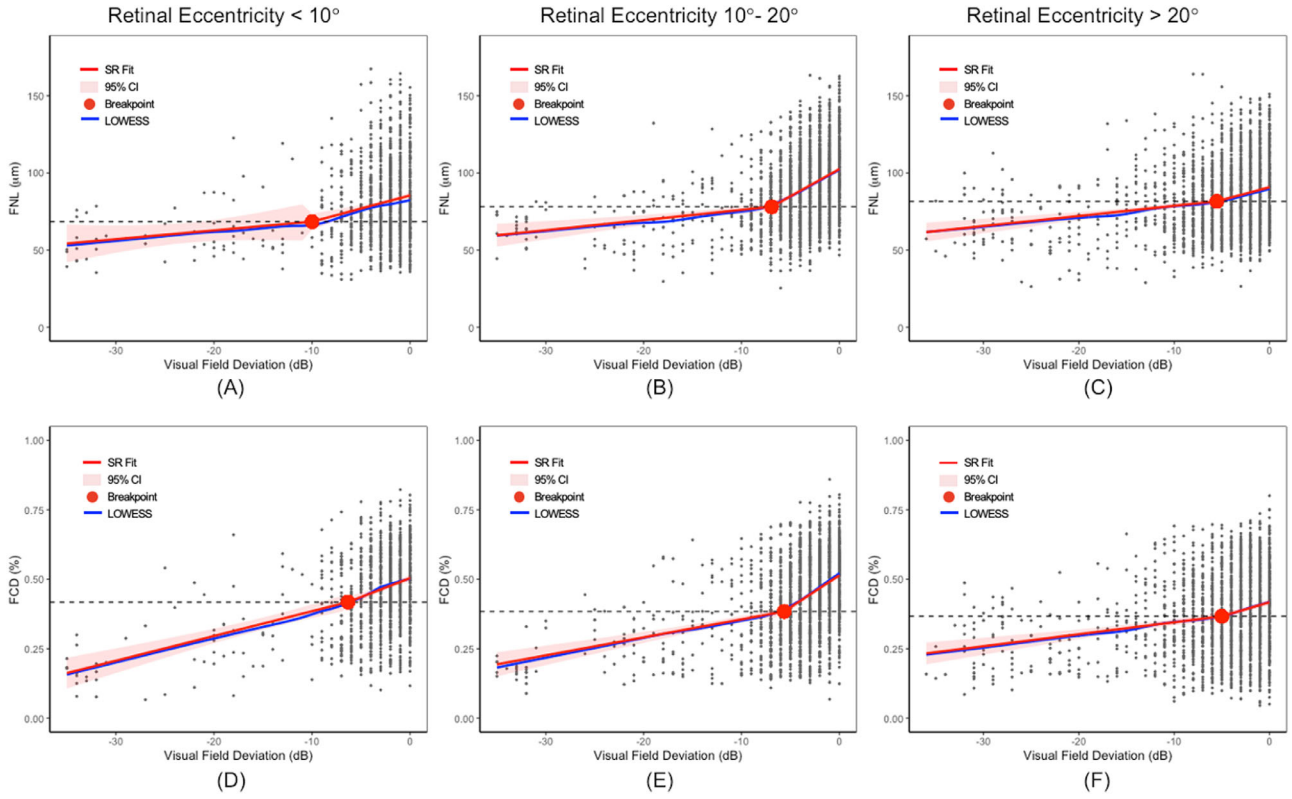

Figure 5. Scatterplots showing the association between VF losses and FCD or focal FNL thickness at different retinal eccentricities. (**A**) FNL thickness against VF loss, eccentricity less than 10°; (**B**) FNL thickness against VF loss, eccentricity between 10° and 20°; (**C**) FNL against VF loss, eccentricity greater than 20°; (**D**) FCD against VF loss, eccentricity less than 10°; (**E**) FCD against VF loss, eccentricity between 10° and 20°; (**F**) FNL thickness against VF loss, eccentricity greater than 20°. LOWESS curves were added to each scatterplot. LOWESS curves (*blue*) are provided with fits obtained from segmented regression analysis (SR, *red*).

Investigative Ophthalmology & Visual Science

Table 4 Predicted Breakpoints and Corresponding Slopes from Segmented Regression Analysis

	VF Breakpoint		Slope Below Breakpoint[†]		Slope Above Breakpoint[‡]		Difference in Slope[§]	
Retinal Eccentricity Zone	**Mean ± SD**	***P*[*]**	**Mean ± SD**	***P***	**Mean ± SD**	***P***	**Mean ± SD**	***P***
0°–10°								
FNL thickness	−10.00 ± 6.14	**0.028**	0.57 ± 0.43	0.183	1.69 ± 0.35	**<0.001**	−1.12 ± 0.55	**0.041**
FCD	−6.33 ± 3.91	0.073	0.89 ± 0.12	**<0.001**	1.36 ± 0.24	**<0.001**	−0.47 ± 0.27	0.081
10°–20°								
FNL thickness	−6.91 ± 0.73	**<0.001**	0.66 ± 0.16	**<0.001**	3.52 ± 0.29	**<0.001**	−2.86 ± 0.33	**<0.001**
FCD	−5.63 ± 0.67	**<0.001**	0.65 ± 0.09	**<0.001**	2.30 ± 0.21	**<0.001**	−1.66 ± 0.22	**<0.001**
20°–30°								
FNL thickness	−5.52 ± 1.72	**0.002**	0.65 ± 0.12	**<0.001**	1.66 ± 0.35	**<0.001**	−1.00 ± 0.37	**0.007**
FCD	−5.00 ± 1.86	**0.008**	0.43 ± 0.08	**<0.001**	1.00 ± 0.23	**<0.001**	−0.57 ± 0.24	**0.017**

Bolded values are statistically significant.
[*] Davies test for existence of a breakpoint.
[†] Slope before breakpoint.
[‡] Slope after breakpoint.
[§] Change in slope after breakpoint.

reported.[17,21–23,38] More focally, the Garway–Heath model[28] has been used to cluster VF locations with the corresponding circumpapillary region into six distinct sectors for sectoral structure–function analysis.[24–26,39] Although the Garway–Heath model is well established, a limitation of the defined clusters is that a more precise structure–functional analysis at the individual test point cannot be demonstrated. In addition, the previous approaches have used standardized definitions of the peripapillary sectors or quadrants for OCT-A analysis and do not account for anatomical individual variations in the relative positions between the optic nerve head and the fovea. These anatomical variations, which have been shown to affect the discriminative ability of peripapillary RNFL measurements in glaucoma,[40–43] are likely attributed to relative shifts in the positions of the nerve fiber bundles and could affect capillary measurements.

An advantage of the focal approach is that we were able to use the actual VF losses at the test locations without averaging over a larger sector. This enabled a more accurate representation of focal changes in the VF, nerve fiber layer thickness, and capillary densities, which could otherwise be obfuscated in a global or sectoral analysis. Results of the focal analyses suggested trends in the disposition of the parameters. Of the VF test locations, FCD and FNL thickness were shown to both be significant in nine test locations which tended temporo-inferiorly, whereas FCD was the significant predictor in 25 locations primarily at the central VF, and FNL thickness was the significant predictor in only seven locations superiorly. Neither FCD nor FNL thickness was a significant predictor in 10 locations, largely in the nasal region. These results suggest that different strategies may be needed for different regions within the VF. VF losses in the central region may be better evaluated with vascular parameters, whereas the peripheral VF may benefit from considering both structural and vascular parameters. The larger influence on vascular measures for the central VF provides some insight on the poorer diagnostic performance in the temporal RNFL compared to the inferior or superior sectors.[44]

Our results show that VF losses at test locations located nearer to fixation were more significantly associated with capillary density than RNFL thickness. Although the analysis was performed on each VF test location individually, it is interesting to note that the results are consistent with previous studies that clustered VF test locations based on the Garway–Heath map. In particular, the individual VF losses significantly associated with capillary density are broadly similar to the temporal, inferotemporal, and superotemporal VF sectors. Our results are comparable to those of Shin et al.,[24] who reported significant associations between VF and vessel density in the inferotemporal and superotemporal sectors in 51 eyes with mild glaucoma (VF MD = −2.32 ± 1.64 dB) only, although we also showed significant associations in the test locations corresponding to the temporal sector. Significant correlations at the inferotemporal and superotemporal sectors were also presented by Rao et al.[27] No significant associations with VF were found for either retinal nerve fiber thickness or capillary density for test locations in the nasal region, which has been shown to have a high degree of variability.[31,45,46] Studies by Kumar et al.[25] and Sakaguchi et al.[26] showed significant associations between VF loss and vascular parameters in more sectors, but this could be attributed to the greater severity of VF loss in those studies, which was consistent with the findings for a group of 40 eyes with severe glaucoma (VF MD = −11.8 ± 5.51 dB) in the same earlier study by Shin et al.[24] The results from the present study provide an indication of the association of vascular and structural parameters with VF loss with respect to eccentricity, which, to the best of our knowledge, has not been shown before using other methods of analysis. Further studies will be needed to evaluate if these conclusions are also applicable to subjects with severe visual loss.

Measures of capillary density from OCT-A may be more useful then RNFL-based measures for the assessment of the structure–functional relationship,[17,21,24,27,37] in particular within 10° of fixation, which largely corresponds to the temporal circumpapillary region. Our results showed that a noticeable floor-like effect was observed at −10 dB for FNL thickness, beyond which there was no appreciable gradient with increasing VF loss, and agree with those of other studies (Hood and Kardon,[3] −10 dB; Mwanza et al.,[7] −10 dB). In contrast, although OCT-A does not provide actual blood flow information, it provides a means of measuring ocular perfusion, which is affected in glaucoma and may be less susceptible to floor effects.[26] This can also be observed in our results by the lack of an apparent floor effect for FCD in all of the zones, in particular within 10° of fixation where no breakpoint was detected. A recent comparison of the measurement floors of capillary density and RNFL thickness in 198 eyes showed similar trends.[8] Although the changepoints were largely lower than in the present study, this could be attributed to the greater severity of glaucoma and the use of global MD rather than focal values. Our results

Investigative Ophthalmology & Visual Science

showed that eccentricity from fixation affects the focal VF relationships, and different strategies may be necessary for visual losses at fixation and at the periphery.

Structural measures showed a floor-like effect for VF test locations in the central 10° of fixation, which corresponds approximately to the temporal circumpapillary region. Similar trends were also observed in the temporal sector in a study by Sakaguchi and colleagues.[26] This could indicate spatial variations in the neuronal component within the RNFL. Although no studies have directly demonstrated this, some studies[7,47] have suggested that the residual floor in the temporal sector is approximately 25% to 30% lower than the superior sector. However, in healthy individuals, the temporal thickness has been reported to be approximately 55% to 60% that of the superior sector.[44,48] Barring astrogliosis, this could imply a lower tolerance for glaucomatous neuronal losses at the temporal sector and an earlier floor effect with the same amount of focal VF loss compared to other sectors. Further studies are necessary to investigate changes in the different components within the RNFL during progression.

Although the results from the present study showed that vascular measures were potentially less susceptible to floor effects than structural measures, repeatability of the vascular measures may pose a potential challenge in monitoring progression. Moghimi and coworkers[8] reported fewer measurable steps from a healthy mean value to a modeled residual floor for OCT-A vascular measures, suggesting that the larger dynamic range of vascular measures was offset by increased measurement variability. Although OCT-A has been demonstrated to have good repeatability in both and normal and diseased eyes,[49,50] other studies have shown that OCT-A measurements can be affected by signal strength[51] and choice of vascular processing approach,[52] as well as physiological characteristics,[53] among other factors. Given these potential sources of variability, these factors should be considered in a progression study, where it may also be advantageous to include baseline parameters.[47]

There are several limitations to our study. Nerve fiber trajectories can traverse across multiple VF test locations in the retina, and unique correspondences between trajectories and test locations can be challenging to determine. However, this is an inherent limitation of VF maps based on fiber tracings in general. The approach we have used mitigates this by using wedge-shaped regions defined by the range of trajectories for each VF location. This enabled a more focal analysis of the VF while providing a reasonable tolerance for variability in the model. An additional outer bound was not imposed to limit the extent of the wedges, but this required quality controls to minimize variations in the optic disc locations. Comparisons were made using only circumpapillary parameters, and the use of retinal capillary density and macular ganglion cell thickness could provide more insight into the structure–function relationship,[8,24,54] particularly with recent widefield retinal imaging protocols. Different machines were used to generate measurements of the RNFL thickness and the OCT-A perfusion parameters, although Tan et al.[55] recently showed that there was excellent agreement between the two machines for RNFL measurement. Most of the subjects in our study had VF MD of better than –6 dB, and evaluation of the structure–function model in subjects with more severe glaucoma was limited. Customized image processing techniques were used for major vessel detection removal and capillary perfusion calculation, which could affect the actual perfusion measurements. Due to the cross-sectional nature of this study, causal relationships could not be evaluated.

In conclusion, capillary density as measured by OCT-A was significantly associated with focal VF losses at a larger number of VF test locations compared to nerve fiber layer measurements from OCT. Capillary densities were also significantly associated with a larger range of VF losses. The findings suggest that capillary density may be useful for modeling focal VF losses in glaucoma. Further studies with longitudinal data are necessary to evaluate the applicability of these findings to glaucoma progression.

Acknowledgments

Supported by Grants from the Singapore National Medical Research Council (CG/C010A/2017, OFLCG/004a/2018, and TA/MOH-000249-00/2018). The sponsor or funding organization had no role in the design or conduct of this research.

Disclosure: **D. Wong**, None; **J. Chua**, None; **E. Lin**, None; **B. Tan**, None; **X. Yao,** None; **R. Chong**, None; **C. Sng**, None; **A. Lau**, None; **R. Husain**, None; **T. Aung**, None; **L. Schmetterer**, None

References

1. Tham YC, Li X, Wong TY, Quigley HA, Aung T, Cheng CY. Global prevalence of glaucoma and projections of glaucoma burden through 2040: a systematic review and meta-analysis. *Ophthalmology*. 2014;121(11):2081–2090.
2. Quigley HA, Broman AT. The number of people with glaucoma worldwide in 2010 and 2020. *Br J Ophthalmol*. 2006;90(3):262–267.
3. Hood DC, Kardon RH. A framework for comparing structural and functional measures of glaucomatous damage. *Prog Retin Eye Res*. 2007;26(6):688–710.
4. Harwerth RS, Wheat JL, Fredette MJ, Anderson DR. Linking structure and function in glaucoma. *Prog Retin Eye Res*. 2010;29(4):249–271.
5. Malik R, Swanson WH, Garway-Heath DF. 'Structure–function relationship' in glaucoma: past thinking and current concepts. *Clin Exp Ophthalmol*. 2012;40(4):369–380.
6. Wollstein G, Kagemann L, Bilonick RA, et al. Retinal nerve fibre layer and visual function loss in glaucoma: the tipping point. *Br J Ophthalmol*. 2012;96(1):47–52.
7. Mwanza JC, Budenz DL, Warren JL, et al. Retinal nerve fibre layer thickness floor and corresponding functional loss in glaucoma. *Br J Ophthalmol*. 2015;99(6):732–737.
8. Moghimi S, Bowd C, Zangwill LM, et al. Measurement floors and dynamic ranges of OCT and OCT angiography in glaucoma. *Ophthalmology*. 2019;126(7):980–988.
9. Danthurebandara VM, Sharpe GP, Hutchison DM, et al. Enhanced structure–function relationship in glaucoma with an anatomically and geometrically accurate neuroretinal rim measurement. *Invest Ophthalmol Vis Sci*. 2014;56(1):98–105.
10. Spaide RF, Fujimoto JG, Waheed NK, Sadda SR, Staurenghi G. Optical coherence tomography angiography. *Prog Retin Eye Res*. 2018;64:1–55.
11. Chua J, Tan B, Ang M, et al. Future clinical applicability of optical coherence tomography angiography. *Clin Exp Optom*. 2019;102(3):260–269.
12. Ang M, Tan ACS, Cheung CMG, et al. Optical coherence tomography angiography: a review of current and future clinical applications. *Graefes Arch Clin Exp Ophthalmol*. 2018;256(2):237–245.
13. Van Melkebeke L, Barbosa-Breda J, Huygens M, Stalmans I. Optical coherence tomography angiography in glaucoma: a review. *Ophthalmic Res*. 2018;60(3):139–151.

14. Rao HL, Pradhan ZS, Weinreb RN, et al. Vessel density and structural measurements of optical coherence tomography in primary angle closure and primary angle closure glaucoma. *Am J Ophthalmol*. 2017;177:106–115.
15. Mansoori T, Sivaswamy J, Gamalapati JS, Balakrishna N. Radial peripapillary capillary density measurement using optical coherence tomography angiography in early glaucoma. *J Glaucoma*. 2017;26(5):438–443.
16. Yarmohammadi A, Zangwill LM, Diniz-Filho A, et al. Relationship between optical coherence tomography angiography vessel density and severity of visual field loss in glaucoma. *Ophthalmology*. 2016;123(12):2498–2508.
17. Liu L, Jia Y, Takusagawa HL, et al. Optical coherence tomography angiography of the peripapillary retina in glaucoma. *JAMA Ophthalmol*. 2015;133(9):1045–1052.
18. Jesus DA, Barbosa Breda J, Van Keer K, Rocha Sousa A, Abegao Pinto L, Stalmans I. Quantitative automated circumpapillary microvascular density measurements: a new angioOCT-based methodology. *Eye (Lond)*. 2019;33(2):320–326.
19. Harris A, Rechtman E, Siesky B, Jonescu-Cuypers C, McCranor L, Garzozi HJ. The role of optic nerve blood flow in the pathogenesis of glaucoma. *Ophthalmol Clin North Am*. 2005;18(3):345–353, v.
20. Flammer J, Orgul S, Costa VP, et al. The impact of ocular blood flow in glaucoma. *Prog Retin Eye Res*. 2002;21(4):359–393.
21. Akagi T, Iida Y, Nakanishi H, et al. Microvascular density in glaucomatous eyes with hemifield visual field defects: an optical coherence tomography angiography study. *Am J Ophthalmol*. 2016;168:237–249.
22. Yarmohammadi A, Zangwill LM, Diniz-Filho A, et al. Peripapillary and macular vessel density in patients with glaucoma and single-hemifield visual field defect. *Ophthalmology*. 2017;124(5):709–719.
23. Richter GM, Sylvester B, Chu Z, et al. Peripapillary microvasculature in the retinal nerve fiber layer in glaucoma by optical coherence tomography angiography: focal structural and functional correlations and diagnostic performance. *Clin Ophthalmol*. 2018;12:2285–2296.
24. Shin JW, Lee J, Kwon J, Choi J, Kook MS. Regional vascular density–visual field sensitivity relationship in glaucoma according to disease severity. *Br J Ophthalmol*. 2017;101(12):1666–1672.
25. Kumar RS, Anegondi N, Chandapura RS, et al. Discriminant function of optical coherence tomography angiography to determine disease severity in glaucoma. *Invest Ophthalmol Vis Sci*. 2016;57(14):6079–6088.
26. Sakaguchi K, Higashide T, Udagawa S, Ohkubo S, Sugiyama K. Comparison of sectoral structure–function relationships in glaucoma: vessel density versus thickness in the peripapillary retinal nerve fiber layer. *Invest Ophthalmol Vis Sci*. 2017;58(12):5251–5262.
27. Rao HL, Pradhan ZS, Weinreb RN, et al. Relationship of optic nerve structure and function to peripapillary vessel density measurements of optical coherence tomography angiography in glaucoma. *J Glaucoma*. 2017;26(6):548–554.
28. Garway-Heath DF, Poinoosawmy D, Fitzke FW, Hitchings RA. Mapping the visual field to the optic disc in normal tension glaucoma eyes. *Ophthalmology*. 2000;107(10):1809–1815.
29. Wang RK, An L, Francis P, Wilson DJ. Depth-resolved imaging of capillary networks in retina and choroid using ultrahigh sensitive optical microangiography. *Opt Lett*. 2010;35(9):1467–1469.
30. Frangi AF, Niessen WJ, Vincken KL, Viergever MA. Multiscale vessel enhancement filtering. In: Wells WM, Colchester A, Delp S , eds. *Medical Image Computing and Computer-Assisted Intervention—MICCAI'98*. Heidelberg: Springer; 1998:130–137.
31. Jansonius NM, Schiefer J, Nevalainen J, Paetzold J, Schiefer U. A mathematical model for describing the retinal nerve fiber bundle trajectories in the human eye: Average course, variability, and influence of refraction, optic disc size and optic disc position. *Exp Eye Res*. 2012;105:70–78.
32. Jansonius NM, Nevalainen J, Selig B, et al. A mathematical description of nerve fiber bundle trajectories and their variability in the human retina. *Vision Res*. 2009;49(17):2157–2163.
33. Hood DC, Zemborain ZZ, Tsamis E, De Moraes CG. Improving the detection of glaucoma and its progression: a topographical approach. *J Glaucoma*. 2009;29(8):613–621.
34. Davies RB. Hypothesis testing when a nuisance parameter is present only under the alternatives. *Biometrika*. 1987;74(1):33–43.
35. Geyman LS, Garg RA, Suwan Y, et al. Peripapillary perfused capillary density in primary open angle glaucoma across disease stage; an optical coherence tomography angiography study. *Br J Ophthalmol*. 2017;101(9):1261–1268.
36. Chen C-L, Zhang A, Bojikian KD, et al. Peripapillary retinal nerve fiber layer vascular microcirculation in glaucoma using optical coherence tomography-based microangiography. *Invest Ophthalmol Vis Sci*. 2016;57(9):OCT475–OCT485.
37. Scripsema NK, Garcia PM, Bavier RD, et al. Optical coherence tomography angiography analysis of perfused peripapillary capillaries in primary open-angle glaucoma and normal-tension glaucoma. *Invest Ophthalmol Vis Sci*. 2016;57(9):OCT611–OCT620.
38. Chen CL, Bojikian KD, Wen JC, et al. Peripapillary retinal nerve fiber layer vascular microcirculation in eyes with glaucoma and single-hemifield visual field loss. *JAMA Ophthalmol*. 2017;135(5):461–468.
39. Rao HL, Kumar AU, Babu JG, Senthil S, Garudadri CS. Relationship between severity of visual field loss at presentation and rate of visual field progression in glaucoma. *Ophthalmology*. 2011;118(2):249–253.
40. Chua J, Schwarzhans F, Nguyen DQ, et al. Compensation of retinal nerve fibre layer thickness as assessed using optical coherence tomography based on anatomical confounders. *Br J Ophthalmol*. 2020;104(2):282–290.
41. Amini N, Nowroozizadeh S, Cirineo N, et al. Influence of the disc-fovea angle on limits of RNFL variability and glaucoma discrimination. *Invest Ophthalmol Vis Sci*. 2014;55(11):7332–7342.
42. Jonas RA, Wang YX, Yang H, et al. Optic disc - fovea angle: the Beijing Eye Study 2011. *PLoS One*. 2015;10(11):e0141771.
43. Resch H, Pereira I, Hienert J, et al. Influence of disc-fovea angle and retinal blood vessels on interindividual variability of circumpapillary retinal nerve fibre layer. *Br J Ophthalmol*. 2016;100(4):531–536.
44. Medeiros FA, Zangwill LM, Bowd C, Vessani RM, Susanna R, Weinreb RN. Evaluation of retinal nerve fiber layer, optic nerve head, and macular thickness measurements for glaucoma detection using optical coherence tomography. *Am J Ophthalmol*. 2005;139(1):44–55.
45. Hong JT, Sung KR, Cho JW, Yun S-C, Kang SY, Kook MS. Retinal nerve fiber layer measurement variability with spectral domain optical coherence tomography. *Korean J Ophthalmol*. 2012;26(1):32–38.
46. Mansoori T, Viswanath K, Balakrishna N. Reproducibility of peripapillary retinal nerve fibre layer thickness measurements with spectral domain optical coherence tomography in normal and glaucomatous eyes. *Br J Ophthalmol*. 2011;95(5):685–688.

Investigative Ophthalmology & Visual Science

47. Kadziauskienė A, Chua J, Baskaran M, et al. Association between structure–function characteristics and visual field outcomes in glaucoma subjects with intraocular pressure reduction after trabeculectomy. *J Glaucoma*. 2020;29(8):648–655.
48. Wong D, Chua J, Baskaran M, et al. Factors affecting the diagnostic performance of circumpapillary retinal nerve fibre layer measurement in glaucoma [published online ahead of print May 5, 2020]. *Br J Ophthalmol*, https://doi.org/10.1136/bjophthalmol-2020-315985.
49. Lei J, Durbin MK, Shi Y, et al. Repeatability and reproducibility of superficial macular retinal vessel density measurements using optical coherence tomography angiography en face images. *JAMA Ophthalmol*. 2017;135(10):1092–1098.
50. Hong J, Tan B, Quang ND, et al. Intra-session repeatability of quantitative metrics using widefield optical coherence tomography angiography (OCTA) in elderly subjects. *Acta Ophthalmol*. 2019;98(5):e570–e578.
51. Lee TH, Lim HB, Nam KY, Kim K, Kim JY. Factors affecting repeatability of assessment of the retinal microvasculature using optical coherence tomography angiography in healthy subjects. *Sci Rep*. 2019;9(1):16291.
52. Tan B, Sim R, Chua J, et al. Approaches to quantify optical coherence tomography angiography metrics. *Ann Transl Med*. 2020;8(18):1205.
53. Müller VC, Storp JJ, Kerschke L, Nelis P, Eter N, Alnawaiseh M. Diurnal variations in flow density measured using optical coherence tomography angiography and the impact of heart rate, mean arterial pressure and intraocular pressure on flow density in primary open-angle glaucoma patients. *Acta Ophthalmol*. 2019;97(6):e844–e849.
54. Smith CA, West ME, Sharpe GP, et al. Asymmetry analysis of macular optical coherence tomography angiography in patients with glaucoma and healthy subjects. *Br J Ophthalmol*. 2020;104(12):1724–1729.
55. Tan B, Chua J, Harish T, et al. Comparison of a commercial spectral-domain OCT and swept-source OCT based on an angiography scan for measuring circumpapillary retinal nerve fibre layer thickness. *Br J Ophthalmol*. 2020;104(7):974–979.

Supplementary Material

Supplementary Video. Video showing the wedges defined by the nerve fibre tracings for each visual field test location.

Investigative Ophthalmology & Visual Science